Growth and properties of high-concentration phases of atomic oxygen on platinum single-crystal surfaces

2008 J. Phys.: Condens. Matter 20 184015

(http://iopscience.iop.org/0953-8984/20/18/184015)

IOP PUBLISHING JOURNAL OF PHYSICS: CONDENSED MATTER

J. Phys.: Condens. Matter **20** (2008) 184015 (11pp) doi:10.1088/0953-8984/20/18/184015

Growth and properties of high-concentration phases of atomic oxygen on platinum single-crystal surfaces

Jason F Weaver[1], **Heywood H Kan and R Bradley Shumbera**

Department of Chemical Engineering, University of Florida, Gainesville, FL 32611, USA

E-mail: weaver@che.ufl.edu

Received 13 July 2007, in final form 30 August 2007
Published 17 April 2008
Online at stacks.iop.org/JPhysCM/20/184015

Abstract

We present results of our recent investigations detailing the growth and properties of oxygen phases prepared on Pt(111) and Pt(100) surfaces in ultrahigh vacuum using oxygen atom beams. Our studies reveal common features in the oxidation mechanisms of Pt(111) and Pt(100). On both surfaces, oxygen atoms initially populate a chemisorbed phase, and then incorporate into intermediate phases prior to the growth of bulk-like oxide. The bulk oxide grows on both surfaces as three-dimensional particles with properties similar to those of PtO_2 and decomposes explosively during heating, exhibiting higher thermal stability than the intermediate oxygen phases. Our results suggest that kinetic barriers stabilize the oxide particles against decomposition, thereby producing explosive desorption, and hence also hinder Pt oxide growth at low coverages. We also find that the kinetics of bulk oxide formation on Pt(100) measured as a function of the O atom incident flux and surface temperature is quantitatively reproduced by a model based on a precursor-mediated mechanism. The model assumes that oxygen atoms adsorbed on top of a surface oxide phase act as a precursor species that can either associatively desorb or react with the surface oxide to produce a bulk oxide particle. Similarities in the development of intermediate oxygen phases on Pt(100), Pt(111) and other transition metal surfaces suggest that precursor-mediated kinetics may be a general feature in transition metal oxidation. Finally, we find that Pt oxide particles are less active than lower-coverage oxygen phases on Pt(111) and Pt(100) toward the oxidation of CO, and that the reaction exhibits autocatalytic kinetics that can be explained with a model that treats the reaction as occurring within a dilute oxygen phase that coexists with oxide particles.

(Some figures in this article are in colour only in the electronic version)

1. Introduction

Understanding the oxidation of Pt and other late transition metals is fundamental to many applications of heterogeneous catalysis, including fuel processing applications, the selective oxidation of organic compounds and pollution control in automobiles. The active surface of a transition metal catalyst can be in an oxidized state at high-pressure reaction conditions, and indeed the extent of surface oxidation can significantly affect catalyst performance since transition metals and their oxides typically possess quite different chemisorptive and reactive properties. Furthermore, oxygen phases or states can exist on transition metal surfaces that are intermediate to a dilute chemisorbed layer and the bulk oxide(s). The possibility that such phases interact uniquely with reactant molecules provides substantial motivation for pursuing a detailed understanding of the oxidation of late transition metal surfaces. Unfortunately, however, challenges in adsorbing high concentrations of oxygen on late transition metal surfaces in ultrahigh vacuum (UHV) have generally limited surface science studies to low coverages of atomic oxygen. As a result, many fundamental aspects of transition metal oxidation have remained unresolved, though recent efforts are illuminating new details.

The difficulty in oxidizing late transition metal surfaces in UHV originates from a kinetic hindrance toward O_2 activation

[1] Author to whom any correspondence should be addressed.

on these surfaces. The probability for O_2 dissociative chemisorption decreases precipitously with atomic oxygen coverage [1, 2] so adsorbing high concentrations of atomic oxygen becomes impractical at the typical O_2 incident fluxes employed in high vacuum. Conducting prolonged O_2 exposures to raise the atomic oxygen coverage is not a viable option because clean-off reactions by background gases begin to occur at comparable rates as O_2 dissociative chemisorption once the atomic oxygen coverage surpasses a certain value. These factors cause Pt single-crystal surfaces to effectively saturate at sub-monolayer atomic oxygen coverages during O_2 dosing in UHV. For example, a maximum atomic oxygen coverage of 0.25 ML (monolayers) is achieved on Pt(111) by dosing with O_2 at typical conditions ($<10^{-6}$ Torr) used in UHV experiments [1]. Indeed, the low reactivity of O_2 toward late transition metal surfaces imposes a significant constraint on surface science studies.

Aggressive approaches must be employed to generate high-concentration oxygen phases on Pt surfaces in UHV and thereby bridge the pressure gap established by the low reactivity of O_2. Dosing with strong molecular oxidants such as NO_2 and O_3 is generally an effective way to adsorb higher atomic oxygen concentrations in UHV than can be attained with O_2. Early work by Koel and co-workers was particularly significant in demonstrating this capability [3–5]. For example, Parker *et al* [5] showed that it is possible to adsorb as much as 0.75 ML of oxygen atoms on Pt(111) by dosing with NO_2 in UHV and then heating the surface to about 500 K to desorb NO. Ozone is a stronger oxidant than NO_2 and can be used to generate even higher atomic oxygen coverages [6]; however, ozone generation and handling is more complicated than NO_2. Other approaches for oxygen adlayer generation include electron- and photon-induced dissociation of chemisorbed O_2 [7] and NO_2 [8], and dosing with gaseous oxygen atoms [9–11]. Finally, UHV systems coupled to a high-pressure cell can be used to generate and characterize high-concentration oxygen phases without exposing the samples to atmospheric gases. This approach has been recently employed in several studies of ordered surface oxides that form on Pd and Rh single-crystal surfaces [12].

In this paper we present recent work from our laboratory in which we have studied the growth and properties of oxygen phases on Pt single-crystal surfaces prepared in UHV using beams of oxygen atoms [10, 13–16]. Since gaseous oxygen atoms are highly reactive, we have been able to cleanly and controllably adsorb high concentrations of atomic oxygen on Pt surfaces, well beyond the concentration at which bulk-like Pt oxide begins to form. This capability has enabled us to examine the mechanisms for oxidation, and the properties of oxygen phases on Pt surfaces in detail using UHV surface diagnostic tools. This paper focuses specifically on the development and properties of oxygen phases on Pt(111) and Pt(100) surfaces, and the reactivity of oxygen phases on these surfaces toward the oxidation of CO.

2. Experimental details

The experiments presented in this paper were conducted in a three-level UHV system that is described in detail elsewhere [17]. Briefly, the top level of the chamber houses a hemispherical analyzer and the necessary excitation sources for investigating solid surfaces using x-ray photoelectron spectroscopy (XPS), Auger electron spectroscopy (AES), electron energy loss spectroscopy (ELS) and low-energy ion scattering spectroscopy (LEISS), as well as for surface cleaning by ion sputtering. The middle level of the chamber is fit with leak valves and a calibrated molecular beam doser [13, 18] that we use in isothermal studies of adsorption and reaction kinetics. The bottom level of the chamber has a four-grid low-energy electron diffraction optics (LEED) and two quadrupole mass spectrometers. Connected to the bottom level of the UHV chamber is also a two-stage differentially pumped beam chamber that houses a plasma source.

We generate O atom beams by partially dissociating pure O_2 in the plasma source located within the differentially pumped beam chamber. Most of the work discussed in this paper utilized a microwave plasma source, but our more recent work on the precursor-mediated oxidation of Pt(100) [16] used an RF plasma source. In each source, gaseous species exit a plasma discharge chamber through a small aperture that directly views the sample surface held in the UHV chamber. The beam first passes through a conical skimmer that separates the first and second pumping stages, and then enters the UHV chamber through a quartz tube, which serves as the final collimating aperture. Electrostatic deflection plates in the first pumping stage remove ions and electrons from the beam, thus ensuring that only neutral species impinge on the samples. From mass spectrometric analysis, we estimate that the plasma-generated beams contain between 5% and 20% O atoms in a balance of O_2 and with negligible quantities of impurities. For a given input power, we find that the RF source is more effective than the microwave source at dissociating O_2. During dosing with the beams, the Pt samples are positioned between 25 and 50 mm from the end of the quartz tube and rotated to an angle of about 45° with respect to the beam axis. We have found that this sample positioning optimizes beam uniformity across the crystal surface.

In our experiments, we used O atom fluxes ranging from approximately 5×10^{12} to 5×10^{13} cm^{-2} s^{-1} at the sample surface. To estimate the O atom incident flux, we perform several short beam exposures ranging from 5 to 20 s to establish an early oxygen uptake curve. The O atom flux is then calculated from the slope of a linear fit to this uptake curve assuming an adsorption probability of unity. We find that the uptake curves on Pt(111) and Pt(100) are well approximated as linear for oxygen coverages up to approximately 0.50 ML, where 1 ML is defined as the density of surface metal atoms for the specific Pt single-crystal surface under study. That we estimate nearly identical beam fluxes using this procedure with different metal surfaces supports the assumption of unit adsorption probability. Furthermore, we find that the fluxes estimated from the uptake procedure agree well with values obtained from a more rigorous approach in which the absolute beam intensity is determined using a calibrated O_2 leak into the chamber [18].

We characterized oxygen phases on Pt(111) and Pt(100) using O_2 temperature programmed desorption (TPD), XPS,

ELS and LEED. We find that TPD is particularly sensitive to the oxygen binding states that populate on the Pt surfaces, and have hence utilized TPD extensively in our investigations of Pt oxidation. All O_2 TPD measurements discussed here began by exposing the sample to the O atom beam, followed by cooling the sample to 300 K at a rate of -3 K s^{-1}, facing the sample toward the entrance of a quadrupole mass spectrometer (QMS) ionizer at a distance of about 10 mm and increasing the sample temperature by a linear rate. Cooling the sample prior to beginning the TPD measurements avoids an initial transient response in the heating by the PID controller, therefore ensuring an approximately linear temperature ramp during the evolution of O_2. Processing the TPD spectra entailed performing a linear background subtraction followed by smoothing with an adjacent averaging procedure.

Absolute coverages of atomic oxygen are determined by calibrating integrated O_2 TPD curves with those obtained from oxygen-covered Pt surfaces prepared by dosing with O_2 to generate known oxygen atom coverages. The dissociative chemisorption of O_2 on Pt(111) effectively saturates at an atomic oxygen coverage of 0.25 ML [1, 7, 19], and a maximum atomic oxygen coverage of 0.63 ML is achieved on Pt(100) by dosing with O_2 with the surface held at 573 K [20]. It is important to mention that we define units of 1 ML for the surface under study so these units differ for Pt(111) versus Pt(100). Specifically, 1 ML is equivalent to 1.51×10^{15} cm^{-2} for Pt(111) [7] and 1.28×10^{15} cm^{-2} for Pt(100) [21].

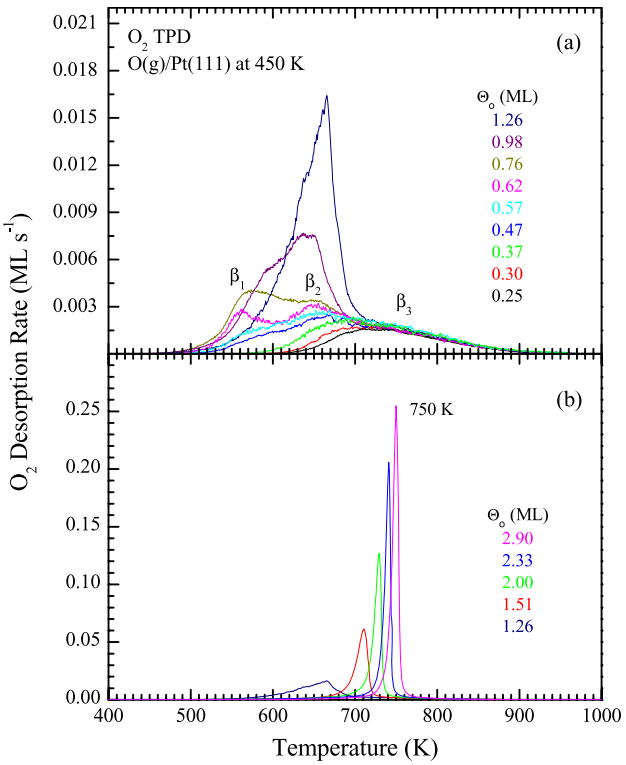

Figure 1. (a) O_2 TPD spectra obtained after exposing Pt(111) at 450 K to an atomic oxygen beam to reach initial oxygen coverages up to 1.3 ML, and (b) initial coverages from 1.3 to 2.9 ML. A heating rate of 3 K s^{-1} was used for each measurement. Notice that the y-axis in (a) is compressed by more than a factor of 10 relative to (b).

3. Results

3.1. Oxidation of Pt(111)

3.1.1. Low-coverage phases. We investigated the oxidation of Pt(111) by gaseous oxygen atoms using TPD, XPS, ELS and LEED [10]. We first discuss the oxygen states that evolve at low coverage, and then present our findings on the development of Pt oxide at higher coverage. Figure 1(a) shows O_2 TPD spectra obtained after preparing relatively low oxygen coverages on Pt(111) held at 450 K. Only a single, broad desorption feature appears in the TPD spectra for oxygen coverages up to 0.25 ML. LEED confirms that this desorption feature arises from oxygen atoms adsorbed in p(2 × 2) domains, consistent with the adlayer structure resulting from dissociation of O_2 [7, 19]. Increasing the oxygen coverage beyond 0.25 ML produces two additional features in the TPD spectra centered at 560 and 650 K, and labeled as β_1 and β_2, respectively. The β_2 feature mainly intensifies as the coverage increases to 0.50 ML, while the β_1 feature intensifies sharply in the coverage range from 0.50 to 0.75 ML.

The intermediate β_1 and β_2 states have been characterized by Koel and co-workers [5] and later in our laboratory [10], yet the exact nature of these states remains unknown. The TPD spectra show that the oxygen–surface binding strength weakens considerably between 0.25 and 0.75 ML. However, photoemission and electron energy loss measurements reveal similar electronic and vibrational properties of oxygen atoms on Pt(111) up to about 0.75 ML [5]. Likewise, the work-function change of Pt(111) increases continuously with oxygen coverage [5], indicating that the average dipole moment per oxygen atom also remains constant throughout the intermediate coverage regime. Finally, at 450 K and below, LEED is unable to identify distinct ordered structures that could be associated with the β_1 and β_2 desorption features. Rather, the (2 × 2) spots from the low-coverage p(2 × 2) structure first become dim as the coverage increases above 0.25 ML, and then the Pt substrate spots fade, indicating that the surface becomes progressively disordered in the intermediate coverage range [5, 10]. The persistence of a (2 × 2) pattern up to 0.50 ML is consistent with a (2 × 2) superstructure in which oxygen atoms occupy both fcc and hcp hollow sites on the Pt(111) surface [7]. Recent TPD experiments using co-adsorbed ^{16}O and ^{18}O atoms on Pt(111) support the idea that oxygen atoms bind at multiple sites above 0.25 ML [22], and hence that the (2 × 2) 'honeycomb' structure is viable. However, DFT calculations appear to refute this idea, as they predict that the fcc site continues to be the preferred binding site for oxygen coverages up to at least 0.50 ML [23].

Another possibility is that Pt–O clusters form on top of the metal surface above 0.25 ML as a result of local restructuring that generates Pt adatoms. Such clusters would disrupt coexisting p(2 × 2) domains and could attenuate electron scattering from the underlying (111) structure, resulting in degradation of the LEED patterns. However, one would expect a lower dipole moment for oxygen incorporated into a cluster compared with chemisorbed oxygen, but this is not supported

by prior work-function measurements [5]. Nevertheless, this interpretation seems plausible considering the growing body of evidence that surface oxides are a common feature in the oxidation of late transition metal surfaces [12]. Interestingly, recent work on Au(111) [8] shows that atomic oxygen adsorption at 200 K produces disordered clusters on top of flat terraces, while annealing at 400 K causes these clusters to agglomerate and order. As discussed below, similar structural changes may occur during Pt(100) oxidation. If disordered Pt–O clusters do exist on Pt(111) above 0.25 ML, these clusters may transform to ordered surface oxide domains at higher temperature that could yield distinct LEED patterns or at least possess structure that can be resolved with scanning tunneling microscopy (STM).

3.1.2. Pt oxide formation on Pt(111). XPS and ELS measurements confirm that a Pt oxide compound forms on the Pt(111) surface above oxygen coverages of about 0.75 ML [10]. The presence of Pt oxide on the surface causes significant changes in the O_2 TPD spectra. As the coverage increases above 0.75 ML, the maximum O_2 desorption rate increases and begins to shift toward higher temperature, causing the desorption curves to undercut the traces obtained at lower coverage (figure 1(a)). The β_1 desorption feature also vanishes as the maximum desorption rate first starts to shift to higher temperature. As the coverage increases above 1.5 ML, desorption becomes explosive as the main peak continues to shift toward higher temperature and intensify dramatically (figure 1(b)). The desorption behavior at high coverage is interesting since it shows that the oxide has a higher thermal stability than the intermediate β_1 and β_2 states, and that the stability of the oxide increases with coverage. The explosive desorption further demonstrates that the oxide on Pt(111) decomposes by a self-accelerating process wherein decomposition occurs at rapidly increasing rates with decreasing oxygen coverage. Explosive desorption can result when three-dimensional clusters decompose since the surface tension increases with decreasing cluster size, causing the clusters to destabilize as they decompose [6, 24]. Based on LEED, oxide formation on Pt(111) destroys the long-range surface order [6, 9, 10], which is consistent with the formation of three-dimensional oxide particles and significant surface restructuring. ELS spectra obtained from oxidized Pt(111) also exhibit a surface plasmon feature that is characteristic of metallic regions present at the vacuum–solid interface, further supporting the conclusion that the oxide grows as three-dimensional particles.

XPS Pt 4f spectra obtained as a function of the oxygen coverage are shown in figure 2. The spectra initially exhibit only slight broadening with increasing oxygen coverage, but a distinct shoulder develops on the high-binding-energy side of the Pt 4f peak as the oxygen coverage increases above about 1 ML. The Pt $4f_{5/2}$ shoulder is centered at approximately 76.9 eV, which is intermediate to the values of 75.6 and 77.4 eV reported for the Pt $4f_{5/2}$ binding energies in bulk PtO and PtO_2 [25–27], respectively, though it is closer to that of PtO_2. While this may indicate the formation of an intermediate oxide such as Pt_3O_4, α-PtO_2 is the thermodynamically preferred

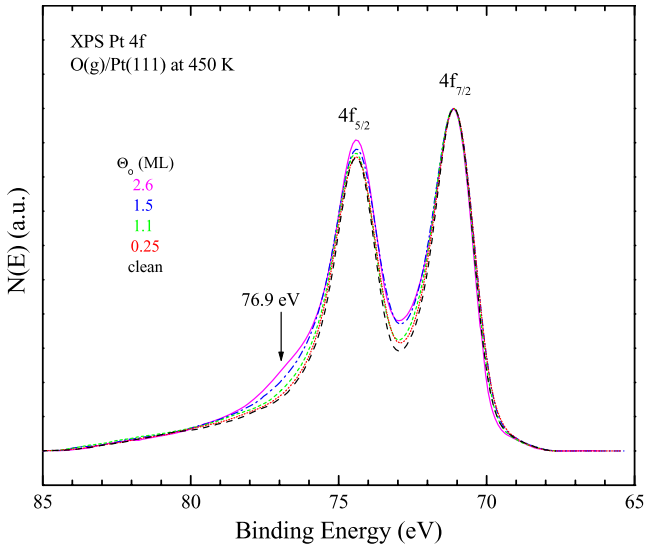

Figure 2. XPS Pt 4f spectra obtained from Pt(111) as a function of the oxygen coverage generated with an oxygen atom beam at a surface temperature of 450 K. Al Kα x-rays were used in each measurement and the hemispherical analyzer was operated in a retarding mode at a pass energy of 27 eV.

form [28]. Thus, we speculate that the oxide on Pt(111) is PtO_2 and either the PtO_2 particles have a high concentration of oxygen vacancies or the underlying metal substrate is effective at screening the final photoexcited state. In either case, the binding energy would be lower than that of bulk PtO_2.

3.1.3. Oxide decomposition kinetics. TPD shows that the oxide on Pt(111) is more thermally stable than the intermediate β_1 and β_2 states, yet the oxide forms only after these intermediate states populate. This suggests that a kinetic hindrance to oxide formation exists at low oxygen coverage, and that the β_1 and β_2 states provide lower energy pathways to oxide formation. Such a kinetic limitation could result if large energy barriers must be overcome for the surface to restructure as oxide particles form. In this interpretation, the intermediate states effectively act as precursors to oxide formation on Pt(111). Note that if the desorption behavior reflected only the thermodynamic stability of the oxygen phases, then one might expect the oxide to form at lower coverage and bypass the less stable β_1 and β_2 states.

We previously employed a so-called island decomposition model to describe the thermal decomposition of oxide particles on Pt(111) [10]. Similar approaches have been successful in describing explosive desorption in other adsorbate/surface systems [29–31], and indeed our use of this model is motivated by the idea that kinetic barriers stabilize the oxide against decomposition. The model assumes that oxygen atoms transfer from the oxide to nearby domains of a dilute phase and that recombinative desorption occurs only from the dilute phase. The implication is that the rate for oxygen recombinative desorption directly from the oxide is much lower than the net rate of oxygen transfer and desorption from the dilute phase. To simplify the model, we assume that oxygen migration is sufficiently rapid to maintain constant oxygen concentrations

within each phase while they coexist. Under these conditions, the total rate of O_2 desorption may be represented by the expressions,

$$\text{for } \Theta_{\text{tot}} \leqslant \Theta_{\text{dp,max}}, \qquad R_{\text{des}} = -\frac{\mathrm{d}\Theta_{\text{tot}}}{\mathrm{d}t} = k_{\text{d}}\Theta_{\text{tot}}^2 \quad \text{and}$$

$$\text{for } \Theta_{\text{tot}} > \Theta_{\text{dp,max}},$$

$$R_{\text{des}} = -\frac{\mathrm{d}\Theta_{\text{tot}}}{\mathrm{d}t} = (1-f)k_{\text{d}}\Theta_{\text{dp,max}}^2 \quad \text{and}$$

$$\Theta_{\text{tot}} = f\Theta_{\text{ox,max}} + (1-f)\Theta_{\text{dp,max}},$$

where Θ_{tot} is the total oxygen coverage, $\Theta_{\text{dp,max}}$ is the maximum coverage of the dilute phase, $\Theta_{\text{ox,max}}$ is the maximum coverage of the oxide phase, f is the fraction of the surface covered by the oxide phase and k_{d} is the rate constant for desorption from the dilute phase. The model assumes that O_2 desorption from the dilute phase is second order in the local oxygen coverage.

We find that the island decomposition model accurately reproduces the main characteristics of the TPD curves observed experimentally for initial coverages above 1.5 ML [10], including the dramatic intensification and shift toward higher temperature of the desorption peak as the initial oxygen coverage increases. This agreement demonstrates that the autocatalytic decomposition of oxidized Pt(111) can be reproduced by a simple model that considers desorption as occurring only from a dilute phase whose area increases during decomposition. In this description, autocatalytic decomposition does not result from an explicit particle size effect but rather follows from the dependence of the desorption rate on the active area for desorption, a condition which holds when oxygen transfer between coexisting phases is sufficiently rapid.

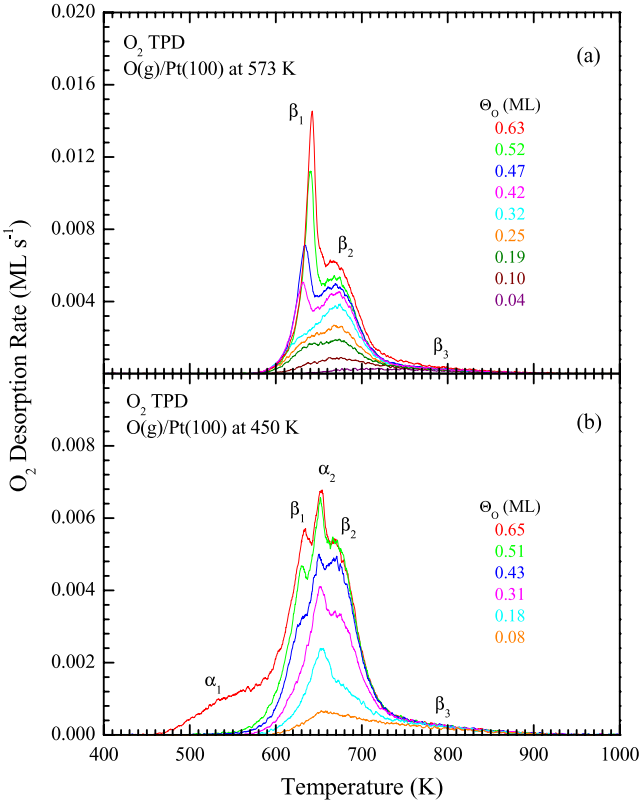

Figure 3. O_2 TPD spectra obtained after exposing Pt(100)-hex-R0.7° to an atomic oxygen beam at surface temperatures of (a) 573 K and (b) 450 K. The initial coverages are stated in the figure and a heating rate of 1 K s^{-1} was used for each measurement. Notice that the y-axis in (a) is expanded by a factor of 2 relative to (b).

3.2. Oxidation of Pt(100)

The oxidation of Pt(100) exhibits similar characteristics to Pt(111). However, through more extensive investigation, we have uncovered new aspects in the oxidation mechanism of Pt(100) not yet discovered for Pt(111). This section will focus on our recent studies of the influence of surface temperature on the development of oxygen phases on Pt(100), the growth and properties of bulk oxide particles and the role of a precursor state in mediating the transition from surface to bulk oxide growth on Pt(100).

3.2.1. Meta-stable oxygen phase. Figure 3(a) shows O_2 TPD spectra obtained from Pt(100) after preparing different oxygen atom coverages at a surface temperature of 573 K. The spectra agree well with TPD spectra obtained after O_2 dissociative chemisorption at 573 K [32–35], suggesting that the evolution of oxygen phases is relatively insensitive to the oxidant at these coverages. Briefly, three states populate nearly sequentially with increasing oxygen coverage at 573 K. Initially, oxygen adsorbs on defect sites associated with the quasi-hexagonal surface reconstruction and gives rises to the small desorption feature labeled β_3. The β_2 desorption feature at approximately 672 K primarily intensifies with increasing coverage from 0.10 to 0.32 ML. Prior studies suggest that this state originates from chemisorbed oxygen atoms arranged into 'disordered' (3 × 1) domains [20]. The assignment of this structure is based on the observation of a faint (3 × 1) LEED pattern after partially desorbing O_2 from a saturated surface to generate an oxygen coverage of 0.40 ML.

The sharp β_1 desorption feature intensifies with increasing coverage above 0.40 ML, its maximum shifting from about 631 to 642 K until the surface effectively saturates at a coverage of 0.63 ML. The LEED pattern obtained from 0.63 ML of oxygen atoms adsorbed at 573 K exhibits clusters of multiple order spots surrounding the $\frac{1}{3}$-order positions [14]. The pattern is relatively dim, but the new spots suggest that the β_1 state is associated with a surface structure that is distinct from the hexagonal reconstruction and the (3 × 1). Previous investigations [20, 33] report similar patterns, described as 'complex', that appear when the β_1 desorption feature becomes prominent in the TPD spectra. Prior measurements also reveal a decrease in the work-function change when the β_1 phase grows on the surface [20], indicating that the O–Pt bonding in this phase involves a more significant in-plane component. The β_1 phase exhibits similar desorption characteristics to the surface oxide phase that forms on Pd(100) over a similar range of oxygen coverage [36, 37]. The structure of the surface oxide on Pd(100) is defined by a $(\sqrt{5} \times \sqrt{5})$-R27° unit cell and produces an intricate LEED pattern [36–39]. Taken together, this information strongly suggests that the β_1 phase on Pt(100) is a surface oxide. That is, the β_1 phase consists of a layer(s)

of Pt and O atoms arranged into a structure that is distinct from the underlying metal substrate.

As seen in figure 3(b), the distribution of oxygen states that evolve with coverage is distinctly different when adsorption occurs at 450 K compared with 573 K. At 450 K, a second desorption feature at approximately 650 K, labeled α_2, intensifies simultaneously with the β_2 feature as the coverage increases from about 0.10 to 0.40 ML. The α_2 feature continues to grow as the β_1 feature evolves from coverages of 0.40 to 0.65 ML. Also, a small desorption feature, labeled α_1, becomes evident at coverages above about 0.50 ML. As discussed in the next section, the α_1 state acts as a precursor to bulk oxide formation at higher coverages [15, 16]. LEED shows only the substrate (1 × 1) pattern in a hazy background at coverages where the α_1 and α_2 states evolve in TPD. It is worth mentioning that this work was the first to identify the α_1 and α_2 states, most likely because prior studies using O_2 as the oxidant were restricted to higher surface temperatures since low O_2 dissociation probabilities and facile clean-off reactions limit the coverages that can be obtained by dosing O_2 at lower temperature.

The α_2 state appears to be a disordered oxygen phase that transforms to the more ordered β_1 phase at a rate that depends on the surface temperature and the oxygen coverage. Formation of the β_1 phase must involve surface restructuring that is more facile at higher surface temperature. The observation that the α_2 state partially replaces the β_1 phase during adsorption at lower surface temperature suggests that the structural changes that produce the β_1 phase are slow at 450 K and, as a result, oxygen atoms become kinetically trapped in the disordered α_2 phase. Most likely, the α_2 desorption feature arises from disordered domains that form as (3 × 1) domains transform to the β_1 surface oxide during oxygen adsorption. Min *et al* [8] report similar behavior for oxygen-covered Au(111) in that disordered clusters form at low temperature but convert to more ordered domains at higher temperature. Recent STM experiments also reveal that an intermediate phase develops on Pd(111) as p(2 × 2) domains transform to the ordered surface oxide [40]. Since the surface oxide (β_1 state) on Pt(100) forms preferentially at higher temperature, and the α_2 phase appears to form under kinetically controlled conditions, we conclude that the α_2 phase is metastable relative to the surface oxide.

3.2.2. Bulk oxide formation on Pt(100). Figure 4 shows O_2 TPD spectra obtained after generating oxygen coverages up to 3.6 ML on Pt(100) at 450 K. The α_1 state intensifies as the coverage increases from about 0.50 to 1 ML and exhibits characteristics of second-order desorption; the α_1 peak maximum shifts slightly toward lower temperature with increasing coverage. Above 1 ML, the α_1 state appears to diminish while a new desorption feature grows and begins to shift toward higher temperature, similar to the behavior observed on Pt(111) (figure 1). The main desorption peak continues to shift toward higher temperature as the coverage further increases, evolving into an explosive desorption feature. XPS and ELS confirm that the onset of explosive desorption coincides with the initial formation of Pt oxide [15].

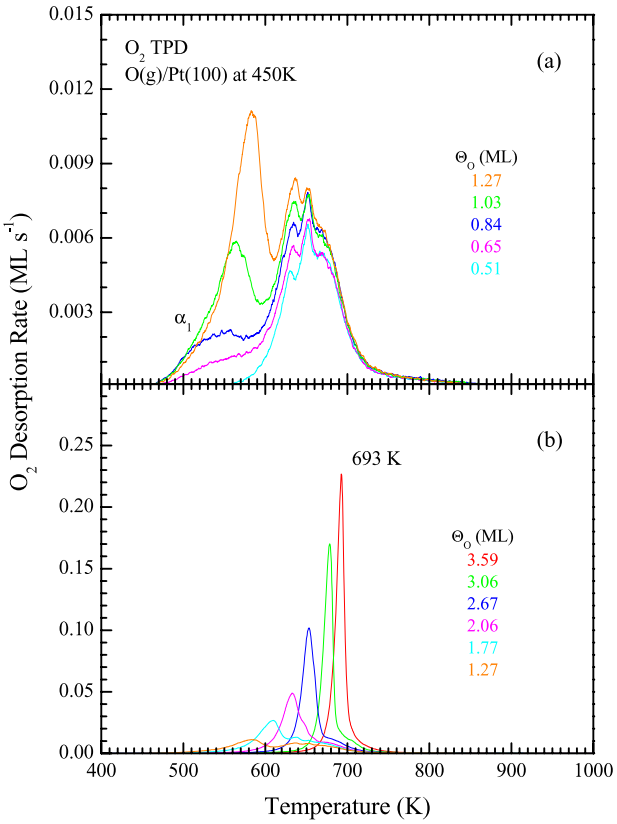

Figure 4. (a) O_2 TPD spectra obtained after exposing Pt(100)-hex-R0.7° at 450 K to an atomic oxygen beam to reach initial oxygen coverages up to 1.3 ML, and (b) initial coverages from 1.3 to 3.6 ML. A heating rate of 1 K s^{-1} was used for each measurement. Notice that the *y*-axis in (a) is compressed by more than a factor of 10 relative to (b).

Interestingly, when the oxygen atom exposure was conducted with the surface held at 573 K, the oxygen coverage reached an apparent saturation of 0.63 ML for the incident beam flux employed ($\Phi_O \sim 3.6 \times 10^{-3}$ ML s^{-1}). Given that the α_1 state desorbs near 550 K in TPD, the apparent saturation at 573 K suggests that the α_1 state must become sufficiently populated for bulk oxide to form on Pt(100), and therefore acts as a precursor to bulk oxide formation.

The bulk oxides that form on Pt(111) and Pt(100) appear to have similar properties for the conditions that were investigated. For example, the XPS Pt $4f_{5/2}$ peak from oxidized Pt(100) exhibits a shoulder centered at roughly 76.9 eV [15], and the ELS spectra from the oxidized Pt surfaces have similar features as well. The Pt 4f shoulder from oxidized Pt(100) does appear to be slightly broader than from Pt(111), possibly indicating a greater fraction of Pt atoms in oxidation states less than +4 on oxidized Pt(100). In fact, recent DFT calculations by Seriani *et al* suggest that the formation of Pt_3O_4 is favorable on the Pt(100) surface [41]. Overall, however, the similarities in the XPS and ELS spectra suggest that the properties of the Pt oxide particles that form on Pt(111) and Pt(100) are largely insensitive to the original geometric structure of the metallic Pt substrate. Despite these similarities, thermal decomposition of nearly the same quantity of oxide on Pt(100) and Pt(111) produces desorption peaks at considerably

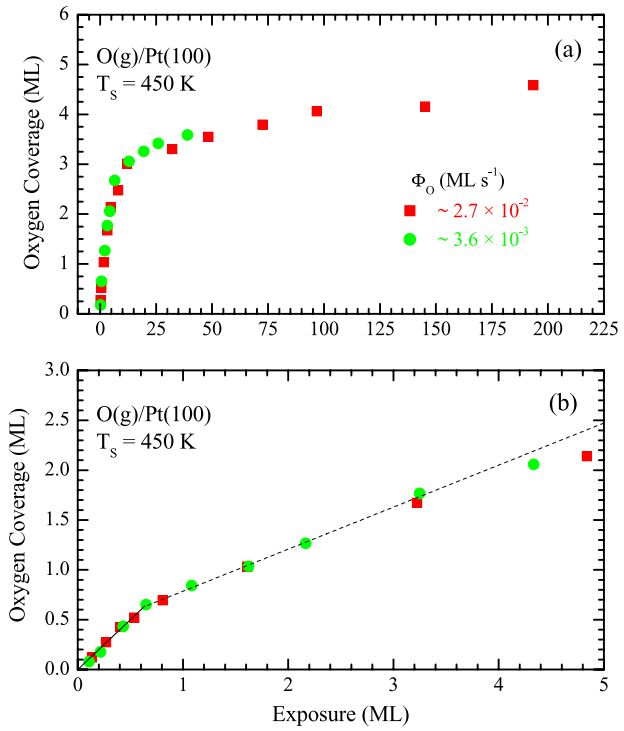

Figure 5. (a) Uptake curves showing the coverages generated on Pt(100) at 450 K as a function of the O atom exposure for different incident fluxes, and (b) a close-up view of the uptake curves for exposures up to 5 ML. The solid and dashed lines represent linear fits to the data over the coverage ranges discussed in the text.

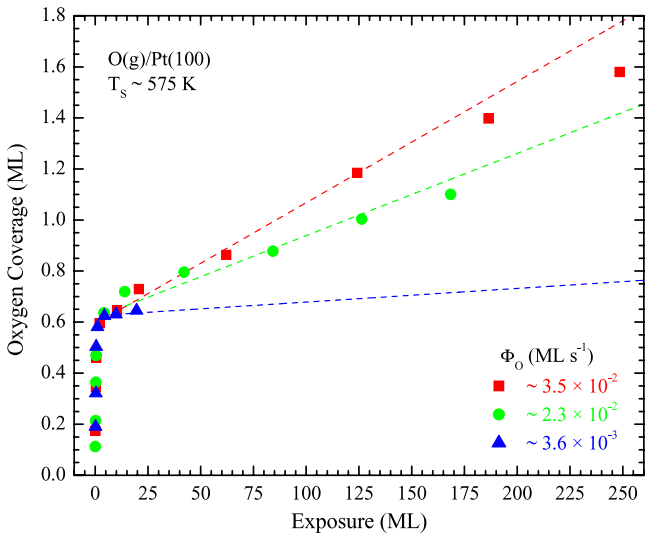

Figure 6. Uptake curves showing the coverages generated on Pt(100) at ∼575 K as a function of the O atom exposure for different incident fluxes. The dashed lines give the predictions of the kinetic model described in the text.

different temperatures of 693 and 750 K, respectively. Taking into account the higher heating rate used in the Pt(111) experiments, Redhead analysis still predicts that the effective activation energy for O_2 desorption is 17 kJ mol^{-1} higher for oxidized Pt(111) than Pt(100). The apparent difference in thermal stability can be explained within the context of the island decomposition model discussed above. According to the model, the O_2 desorption rate during oxide decomposition occurs only from a dilute phase that coexists with the oxide, with this dilute phase resembling domains of oxygen atoms chemisorbed on the metal substrate. Comparison of the TPD spectra shows that chemisorbed oxygen atoms desorb at lower temperature from Pt(100) compared with Pt(111). Thus, it is reasonable to conclude that oxide particles with similar properties do form on Pt(111) and Pt(100), but that the oxide on Pt(100) is less thermally stable due to more facile desorption of chemisorbed oxygen from this surface.

3.2.3. Precursor-mediated bulk oxide formation. The α_1 state appears to serve as a precursor to bulk oxide formation on Pt(100). To further probe the nature of the α_1 state, we prepared a saturated surface oxide phase (β_1 state) at 573 K, and then exposed the sample to the O atom beam at 450 K for several minutes. This treatment results in substantial population of the α_1 state, indicating that formation of the α_1 state does not require the meta-stable α_2 state to be present on the surface. The α_1 state therefore appears to be associated with the surface oxide since the α_1 state populates when the surface oxide initially covers the surface. Assuming that oxygen atoms do not readily penetrate the surface oxide, we speculate that the α_1 state corresponds to oxygen atoms adsorbed on top of the surface oxide. Considering the uptake data discussed above, we further hypothesized that a reaction between the surface oxide and oxygen atoms adsorbed on top of the surface oxide initiates the formation of bulk oxide particles on Pt(100) [15].

To examine the role of the precursor state in more detail, we recently investigated the oxidation kinetics of Pt(100) as a function of the surface temperature and the O atom beam flux [16]. Figures 5 and 6 show oxygen uptake curves, displayed as oxygen atom coverage versus oxygen atom exposure, for oxidation conducted at surface temperatures of 450 and ∼575 K, respectively, and different incident fluxes, spanning about an order of magnitude range. As seen in figure 5(a), the uptake at 450 K is initially rapid, and slows down significantly only as the coverage increases above 2.5 ML. The uptake curves at 450 K are also independent of the incident O atom flux for the overlapping coverages that were examined (up to ∼3.5 ML). Since the slope of the uptake curve is equivalent to

$$\frac{\partial[\mathrm{O}]}{\partial \varepsilon} = \frac{R}{\Phi_{\mathrm{O}}},$$

where [O], ε, R and Φ_{O} represent the total coverage, the exposure in ML, the uptake rate and the O incident flux, respectively, the flux independence of the uptake curves indicates that the uptake rate at 450 K depends linearly on the incident flux.

Close inspection of the uptake curves obtained at 450 K also reveals a sudden decrease in the uptake rate at a coverage of about 0.60 ML, suggesting a change in the predominant mechanism for oxygen uptake. As seen in figure 5(b), the oxygen coverage rises linearly with exposure up to [O] ∼ 0.60 ML, and thereafter continues to increase linearly but only

at about 40% of the initial rate. The linear increase continues to a coverage of about 1.7 ML at which point the uptake rate decreases again. The linearity of the uptake curve for coverages from about 0.60 to 1.7 ML suggests that a given mechanism governs the uptake of oxygen atoms on Pt(100) over the coverage regime at which bulk oxide particles begin to form at 450 K.

At 575 K and early exposure, the oxygen coverage increases rapidly with exposure, and the uptake curve is independent of the incident flux (figure 6). The uptake curves then exhibit an abrupt decrease in slope at a coverage of about 0.60 ML, and thereafter continue to rise linearly with exposure up to an oxygen coverage of at least 1.6 ML. This behavior is similar to that observed at 450 K, but the oxidation rate is much slower at 575 K. Another key difference is that the slopes of the uptake curves at 575 K increase with increasing incident flux above a coverage of 0.60 ML. This indicates that the uptake rate at 575 K increases non-linearly with flux above a critical coverage. Finally, we find that for a given exposure the oxygen coverage increases slightly with increasing surface temperature from 450 to 475 K, but then decreases with increasing surface temperature above 475 K [16]. Indeed, a decrease in the oxidation rate with surface temperature is characteristic of a precursor-mediated process. Overall, the measured rate behavior suggests that different reaction steps control the rate of oxide formation in the limits of low and high surface temperature, respectively.

3.2.4. Kinetic model and analysis. We find that a simple model based on a precursor-mediated mechanism quantitatively reproduces the oxidation kinetics in the early stages of bulk oxide formation. The following kinetic scheme depicts the reaction steps considered in the model,

$$\text{(a)} \quad \mathrm{O(g)} \rightarrow \mathrm{O(ad)}$$

$$\text{(d)} \quad \mathrm{2O(ad)} \rightarrow \mathrm{O_2(g)}$$

$$\text{(r)} \quad x\mathrm{O(ad)} + \text{surface oxide} \rightarrow \text{bulk oxide.}$$

Here, steps (a) and (d) represent the adsorption of a gas-phase O atom into the precursor state and the associative desorption of O atoms from the precursor, respectively. Step (r) represents the reaction between the oxide precursor and the surface (2D) oxide to form a bulk (3D) oxide particle. We assume that the rate of O atom adsorption into the precursor state is given by the equation, $r_a = \Phi_O S_{2D}$, where S_{2D} is the probability that an incident O atom will adsorb onto the 2D oxide. This expression assumes that the adsorption probability is independent of the precursor coverage, which is reasonable given the linearity of the uptake curves in the regime of initial oxide formation (figure 5(b)). Also, by assuming that the desorption and reaction rates follow power law forms, the rates for reaction steps (d) and (r) may be written as $r_d = k_d\Theta^m$ and $r_r = k_r\Theta^n$, respectively, where k_d and k_r denote the rate coefficients for these reactions and Θ is the surface concentration of precursor O atoms.

To derive analytic expressions for the oxidation rate, we consider the kinetics in the limits of low and high surface temperature, and assume that the coverage of the precursor species reaches a steady value during uptake. Firstly, we consider that at sufficiently low surface temperature the rate of precursor desorption becomes much smaller than the reaction rate, or $r_d \ll r_r$. This follows from the observation that the precursor state desorbs in TPD at about 550 K whereas oxide formation occurs at temperatures as low as 100 K [42]. Thus, in the limit of low surface temperature, the reaction rate is approximately equal to the rate of adsorption, or $r_r \approx r_a = \Phi_O S_{2D}$. In this case, the uptake rate depends linearly on the incident flux so uptake curves obtained at different fluxes should overlap when plotted as coverage versus exposure, exactly as observed for the uptake data obtained at 450 K (figure 5). In fact, the dashed line in figure 5(b) shows that for coverages from about 0.60 to 1.7 ML the uptake curves are very well approximated by a single line with a slope of $S_{2D} = 0.42$. Furthermore, since O atoms are highly reactive, the probability for O atom adsorption should depend only weakly on the surface temperature. The weak surface temperature dependence of the oxidation rate in the low-temperature limit is consistent with this expectation.

At high surface temperatures, the rate of precursor desorption exceeds that of reaction, or $r_d \gg r_r$. Thus, a quasi-equilibrium between adsorption and desorption establishes the coverage of precursor O atoms in the high-temperature limit, and the following expression for the reaction rate results,

$$r_r \approx k_r \left(\frac{\Phi_O S_{2D}}{k_d} \right)^{n/m}.$$

Since the precursor species desorbs near 550 K in TPD, the high-temperature limit should apply to the uptake data obtained at 575 K. It is possible to estimate the ratio n/m by noticing that the model predicts the following relationship,

$$\left(\frac{\partial \ln [\mathrm{O}]_{3D}}{\partial \ln \Phi_O} \right)_{t,T_S} = \frac{n}{m},$$

where $[\mathrm{O}]_{3D}$ is the coverage of the 3D oxide, estimated as the total coverage less the saturation value for the surface oxide of 0.63 ML [20], and the derivative performed at constant exposure time and surface temperature (575 K). After analyzing the data, we find that $n/m \approx 2$. Thus, $n \approx 4$ if the desorption of precursor O atoms follows second-order kinetics as suggested previously [15]. The fourth-order dependence is interesting since it implies a critical configuration for oxide nucleus formation requiring four adsorbed oxygen atoms. This finding may help guide computational efforts directed toward elucidating the atomic-level processes involved in the transition from surface to bulk oxide growth on Pt(100).

Given $n/m \approx 2$, it is also possible to evaluate effective kinetic parameters from the temperature dependent data (not shown). Assuming an Arrhenius form for the rate coefficients k_d and k_r, the effective pre-exponential factor and activation energy for oxide particle formation are given by ν_r/ν_d^2 and $(E_r - 2E_d)$, respectively, in the high-temperature limit. Here, ν_r and E_r represent the pre-exponential factor and activation energy for step (r), while ν_d and E_d are the pre-exponential factor and activation energy for step (d). Likewise, the

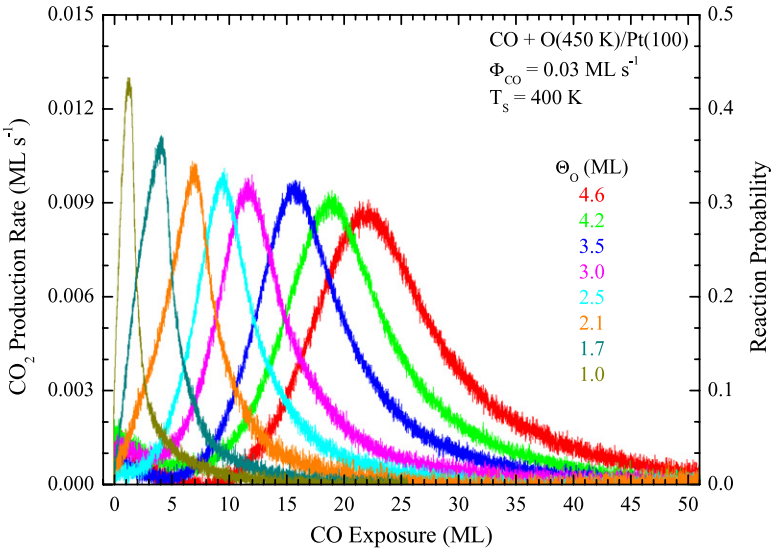

Figure 7. Rate of CO_2 production as a function of CO beam exposure to O-covered Pt(100) measured at $T_s = 400$ K for initial atomic oxygen coverages ranging from 1 to 4.6 ML.

expression for r_r can be rewritten as

$$r_r = \left(\frac{\nu_r}{\nu_d^2}\right)(\Phi_O S_{2D})^2 \exp\left[\frac{-(E_r - 2E_d)}{RT_S}\right].$$

From uptake data obtained as a function of the surface temperature, we estimate that $(E_r - 2E_d) = -102.6$ kJ mol^{-1} and $\nu_r/\nu_d^2 = 1.8 \times 10^{-10}$ s ML^{-1}. Using these values, and $S_{2D} = 0.42$, the model predicts the dashed lines shown in figure 6. Indeed, the model predictions agree closely with the experimental data, deviating by at most 15% at high coverages.

The precursor-mediated model quantitatively reproduces the measured kinetics of initial bulk oxide formation on Pt(100), and provides a simple explanation of the predominant rate processes involved in the transition to bulk oxide growth. According to the model, the observed change in the flux and surface temperature dependence of the oxidation rate is due to a change in the rate-controlling steps for bulk oxide formation from reaction at low temperature to precursor desorption at high temperature. It is interesting that other late transition metal surfaces exhibit similar oxidation behavior to Pt(100). For example, TPD data (figure 1) suggests that a precursor state populates on Pt(111) prior to the growth of oxide particles. We have also recently observed desorption behavior from Pd(111) that is qualitatively similar to that of the Pt surfaces in that a low-temperature feature evolves in the O_2 TPD and then vanishes as bulk-like PdO forms. These similarities suggest that precursor-mediated kinetics is a general feature in the oxidation of late transition metal surfaces. If validated, this finding should facilitate the development of predictive models of transition metal oxidation.

3.3. CO oxidation on oxidized Pt surfaces

We conclude this paper by presenting recent results on the reactivity of oxygen phases on Pt surfaces toward the oxidation of CO. As is well known, CO oxidation is a prototypical reaction for UHV investigations and is an important reaction in the catalytic remediation of exhaust gases from automobiles. Understanding the oxidation of CO in the presence of high-coverage surface oxygen phases is particularly important to Pt-based catalysis performed under oxygen-rich conditions such as in lean-burn engines. In recent work, we have used temperature programmed reaction spectroscopy (TPRS) and beam reflectivity measurements to study CO oxidation on Pt(111) [13] and Pt(100) at initial oxygen coverages up to 4.6 ML, which we generate in UHV using O atom beams.

A general finding from this work is that bulk-like Pt oxide is less active toward CO oxidation than are oxygen phases that exist at lower coverage. This may be seen from isothermal measurements of the CO_2 production rate as a function of the initial oxygen coverage on Pt(100) (figure 7). In these measurements, oxygen-covered Pt(100) was held at 400 K and exposed to a CO molecular beam while the CO_2 partial pressure was simultaneously monitored. The data shows that the initial reaction rate generally decreases and longer times elapse prior to the maximum reaction rate as the initial oxygen coverage increases from 1 to 4.6 ML. The same trend is observed for oxygen coverages below 1 ML on Pt(100), and also for CO oxidation on Pt(111) [13]. This behavior demonstrates that the consumption of oxide particles by reaction enhances the surface reactivity toward CO oxidation.

TPRS experiments suggest that limited adsorption of CO is responsible for the low reactivity of oxidized Pt(111) and Pt(100). In these experiments, the oxidized Pt surfaces were held at 100 K and then exposed to doses of CO well in excess of that needed to saturate the clean surfaces. During subsequent TPRS experiments, we observe CO desorption below 200 K and a small amount of CO_2 that slowly evolves from the surface in a broad feature, extending from about 200 to 530 K, that rises only slightly above the baseline. The slow production of CO_2 in these experiments is consistent with a small fraction of the CO reacting on low-coverage oxygen domains and

defect sites that exist on the partially oxidized surfaces. The TPRS results further reveal that CO binds weakly on the Pt oxide particles. As a result, the concentration of CO must remain very low on the oxide particles under the conditions examined in the isothermal measurements, which causes the CO oxidation rate to also remain low.

The CO oxidation kinetics on the partially oxidized Pt surfaces is consistent with a mechanism wherein CO molecules adsorb and react only on domains of a dilute oxygen phase that coexist with oxide particles, and with the oxide particles supplying oxygen atoms to the dilute phase for reaction. This reaction mechanism is autocatalytic because the total reaction rate is proportional to the area covered by the dilute phase, and this area increases as oxide particles are consumed during reaction. The mechanism is qualitatively similar to the island decomposition model used to describe explosive O_2 desorption from Pt(111) [10]. We used this reaction model to simulate the CO_2 production rate as a function of the CO exposure to partially oxidized Pt(111). For a detailed description of the model, the reader is referred to [13]. Briefly, the model assumes that reaction occurs on a dilute phase on which the maximum oxygen coverage is 0.75 ML, which corresponds to the onset of oxide formation [10], and employs kinetic parameters for CO adsorption and reaction on this phase that are mostly taken from the literature. The CO adsorption probability is treated as a decreasing function of the oxygen coverage on the dilute phase, and the rate of oxygen migration from the oxide to the dilute phase is assumed to scale with $f^{1/2}$, where f represents the fractional area of the surface covered by oxide domains.

As illustrated in figure 8, the model accurately reproduces the main characteristics of the experimental CO_2 production rate curves obtained at 400 K and high initial oxygen coverages. For example, the model predicts rate curves with similar shapes and intensities as the experimental curves. The simulations also correctly predict that the time delay prior to the rate maximum increases with the initial oxygen coverage, though the predicted time delays are longer than observed experimentally. We find, however, that the computed time delays are very sensitive to the initial oxygen coverage so error in the initial coverage used in the calculation greatly accentuates the difference between the simulated and experimental time delays. Despite this difference, the overall agreement between the model and experimental data is good, implying that the model captures the key mechanistic features of CO oxidation on partially oxidized Pt(111).

Although our findings contribute to the understanding of CO oxidation at realistic conditions, it is important to recognize that the reactive behavior of Pt surfaces may differ in the presence of high partial pressures of CO and O_2. For example, it is possible that O_2 molecules chemisorbed on Pt oxide domains play a role in CO oxidation at high O_2 pressures, possibly enhancing the reactivity of the oxide. In fact, preliminary data from our laboratory suggests that O_2 molecules can bind more strongly on oxidized Pt and Pd surfaces compared with the clean metals, which means that the instantaneous O_2 surface coverage would be higher on the oxidized surfaces in the presence of gaseous O_2. Possibilities

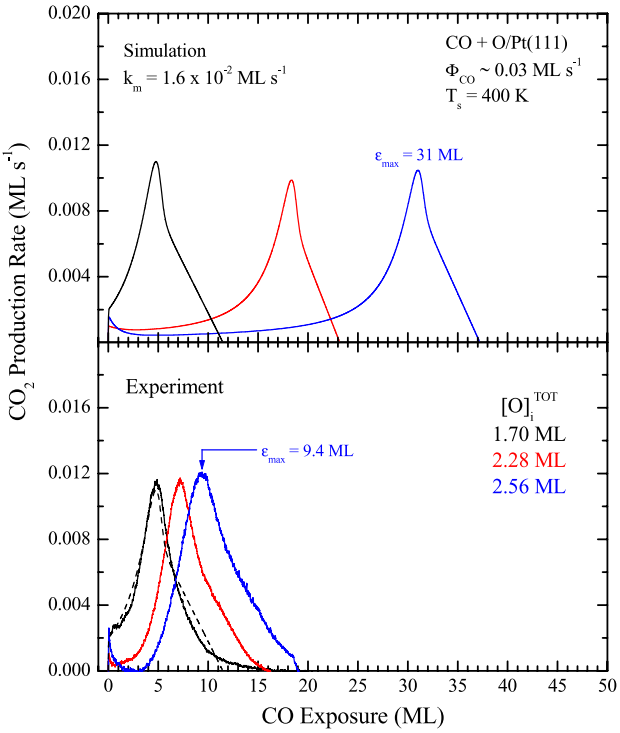

Figure 8. Rate of CO_2 production as a function of CO beam exposure to O-covered Pt(111) obtained experimentally (bottom) and simulated (top) using the kinetic model discussed in the text. The rate curves are obtained at a surface temperature of 400 K and initial atomic oxygen coverages of 1.7, 2.28 and 2.56 ML. The dashed line is the rate curve simulated using an initial coverage of 1.7 ML.

such as this highlight the need to characterize any alternate pathways or processes that become accessible, and potentially dominant, at commercially relevant pressures.

4. Summary

Using beams of oxygen atoms, we have oxidized Pt single-crystal surfaces in UHV, and investigated the growth and properties of the resulting oxygen phases using surface analysis techniques. The oxidation of Pt(111) and Pt(100) exhibit common characteristics in that oxygen atoms initially chemisorb into a dilute layer, and then incorporate into intermediate phases prior to the growth of bulk-like Pt oxide particles. The intermediate regime appears to involve the formation of surface oxide domains followed by oxygen atom adsorption on top of the surface oxide. Meta-stable phases can also develop when surface oxide formation is kinetically limited. Additional investigations to probe the surface structure will help to further clarify the properties of the intermediate phases. We find that the kinetics governing bulk oxide formation on Pt(100) measured as a function of the incident O atom flux and surface temperature is quantitatively reproduced by a model based on a precursor-mediated mechanism. The model assumes that oxygen atoms adsorbed on top of a surface oxide act as a precursor species that can either associatively desorb or react with the surface oxide to produce bulk oxide. Similarities in the oxygen phase development

among late transition metal surfaces suggest that precursor-mediated kinetics may be a general feature in transition metal oxidation. On both Pt(111) and Pt(100), bulk oxide grows as three-dimensional particles with properties similar to those of PtO_2. The oxide particles decompose explosively during heating, exhibiting higher thermal stability than the intermediate oxygen phases. The oxide decomposition kinetics is consistent with the conclusion that kinetic barriers stabilize the oxide particles against thermal decomposition, and hence also hinder oxide particle formation at low coverage.

Finally, we find that Pt oxide particles are less active than lower-coverage oxygen phases on Pt(111) and Pt(100) toward the oxidation of CO, and that the reaction kinetics on the partially oxidized Pt surfaces is autocatalytic. TPRS results suggest that the low reactivity originates from a limitation to CO adsorption on the Pt oxide. While our studies provide new insights for understanding the growth and properties of high-concentration oxygen phases on Pt surfaces, we emphasize the importance of continuing efforts to develop instrumentation and methodologies that enable *in situ* studies of gas–solid interactions at high-pressure reaction conditions. Such studies will provide a stringent test of UHV methods designed to simulate key aspects of the high-pressure environment, and are essential for elucidating alternate reaction pathways or processes that may become accessible under realistic reaction conditions.

Acknowledgments

We gratefully acknowledge financial support for this work provided by the Department of Energy, Office of Basic Energy Sciences, Catalysis and Chemical Transformations Division through grant number DE-FG02-03ER15478. JFW is also grateful for financial support provided by NSF-CAREER award CTS-0348287.

References

[1] Campbell C T, Ertl G, Kuipers H and Segner J 1981 *Surf. Sci.* **107** 220
[2] Luntz A C, Williams M D and Bethune D S 1988 *J. Chem. Phys.* **89** 4381
[3] Banse B A and Koel B E 1990 *Surf. Sci.* **232** 275
[4] Parker D H and Koel B E 1990 *J. Vac. Sci. Technol.* A **8** 2585
[5] Parker D H, Bartram M E and Koel B E 1989 *Surf. Sci.* **217** 489
[6] Saliba N, Tsai Y L, Panja C and Koel B E 1999 *Surf. Sci.* **419** 79
[7] Steininger H, Lehwald S and Ibach H 1982 *Surf. Sci.* **123** 1
[8] Min B K, Alemozafar A R, Biener M M, Biener J and Friend C M 2005 *Top. Catal.* **36** 77
[9] Parkinson C R, Walker A and McConville C F 2003 *Surf. Sci.* **545** 19
[10] Weaver J F, Chen J J and Gerrard A L 2005 *Surf. Sci.* **592** 83
[11] Li W X, Osterlund L, Vestergaard E K, Vang R T, Matthiesen J, Pedersen T M, Laegsgaard E, Hammer B and Besenbacher F 2004 *Phys. Rev. Lett.* **93** 146104
[12] Lundgren E, Mikkelsen A, Andersen J N, Kresse G, Schmid M and Varga P 2006 *J. Phys.: Condens. Matter* **18** R481
[13] Gerrard A L and Weaver J F 2005 *J. Chem. Phys.* **123** 224703
[14] Shumbera R B, Kan H H and Weaver J F 2006 *Surf. Sci.* **600** 2928
[15] Shumbera R B, Kan H H and Weaver J F 2007 *Surf. Sci.* **601** 235
[16] Shumbera R B, Kan H H and Weaver J F 2007 *Surf. Sci.* **601** 4809
[17] Gerrard A L, Chen J J and Weaver J F 2005 *J. Phys. Chem.* B **109** 8017
[18] Gerrard A L 2005 *Interactions of Atomic Oxygen with Pt(111) and Nitrided Si(100)* (Gainesville, FL: University of Florida)
[19] Gland J L, Sexton B A and Fisher G B 1980 *Surf. Sci.* **95** 587
[20] Griffiths K, Jackman T E, Davies J A and Norton P R 1984 *Surf. Sci.* **138** 113
[21] Norton P R, Davies J A, Creber D K, Sitter C W and Jackman T E 1981 *Surf. Sci.* **108** 205
[22] Jerdev D I, Kim J, Batzill M and Koel B E 2002 *Surf. Sci.* **498** L91
[23] Tang H R, Van der Ven A and Trout B L 2004 *Phys. Rev.* B **70** 045420
[24] Campbell C T 1997 *Surf. Sci. Rep.* **27** 1
[25] Bancroft G M, Adams I, Coatsworth L L, Bennewitz C D, Brown J D and Westwood W D 1975 *Anal. Chem.* **47** 586
[26] Barr T L 1978 *J. Phys. Chem.* **82** 1801
[27] Jung M-C, Kim H-D, Han M, Jo W and Kim D C 1999 *Japan. J. Appl. Phys.* **38** 4872
[28] Samsonov G V (ed) 1973 *The Oxide Handbook* (New York: IFI/Plenum) Translated from Russian by C N Turton and T I Turton
[29] Skelly J F, Bertrams T, Munz A W, Murphy M J and Hodgson A 1998 *Surf. Sci.* **415** 48
[30] Klier K, Wang Y-N and Simmons G W 1993 *J. Phys. Chem.* **97** 633
[31] Klötzer B, Hayek K, Konvicka C, Lundgren E and Varga P 2001 *Surf. Sci.* **482–485** 237
[32] Kneringer G and Netzer F P 1975 *Surf. Sci.* **49** 125
[33] Barteau M A, Ko E I and Madix R J 1981 *Surf. Sci.* **102** 99
[34] Norton P R, Griffiths K and Bindner P E 1984 *Surf. Sci.* **138** 125
[35] Guo X C, Bradley J M, Hopkinson A and King D A 1994 *Surf. Sci.* **310** 163
[36] Chang S-L and Thiel P A 1988 *J. Chem. Phys.* **88** 2071
[37] Zheng G and Altman E I 2002 *Surf. Sci.* **504** 253
[38] Lundgren E, Gustafson J, Mikkelsen A, Andersen J N, Stierle A, Dosch H, Todorova M, Rogal J, Reuter K and Scheffler M 2004 *Phys. Rev. Lett.* **92** 046101
[39] Kostelnik P, Seriani N, Kresse G, Mikkelsen A, Lundgren E, Blum V, Sikola T, Varga P and Schmid M 2007 *Surf. Sci.* **601** 1574
[40] Gabasch H, Unterberger W, Hayek K, Klotzer B, Kresse G, Klein C, Schmid M and Varga P 2006 *Surf. Sci.* **600** 205
[41] Seriani N, Pompe W and Ciacchi L C 2006 *J. Phys. Chem.* B **110** 14860
[42] Kan H H, Shumbera R B and Weaver J F 2007 *J. Chem. Phys.* **126** 134704